# Chapter 8
# Droplet Impact on a Solid Surface

**Abstract** This chapter considers droplet-wall interaction and droplet impact and splashing on a solid surface. The discussion on droplet-wall interaction considers thermo-fluid-dynamic processes associated with droplet impact onto solid surfaces. The emphasis is put on the disintegration mechanisms as an introduction to the intricate interaction phenomena occurring at spray impingement. The analysis starts with the simplest situation of single droplet impacts onto non-heated and dry surfaces; further complexities are then introduced which consider the interaction with a liquid film and the combined effects of heat transfer. The discussion on droplet impact and splashing on a solid surface includes splashing and fragmentation of molten metal and other liquid droplets landing on a solid surface. Issues such as different types of splashing, corona splashes, freezing induced splashing are considered from an experimental point of view.

**Keywords** Droplet impact · Spread · Disintegration · Disintegration limits · Secondary atomization · *Wettability* · Surface topography · Heat transfer regimes · Thermal induced atomization · Molten metal droplet impact · Corona splashes



N. Ashgriz (ed.), *Handbook of Atomization and Sprays*,
DOI 10.1007/978-1-4419-7264-4_8, © Springer Science+Business Media, LLC 2011

# Droplet–Wall Interactions

António L.N. Moreira and A.S. Moita

## Single Droplet Impingement onto Non-heated Dry Surfaces

### *The Impact Regimes*

When a droplet impacts onto a solid surface, different outcomes may arise depending on the dynamics of the interactions occurring at the liquid-solid interface which, for impacts onto cold, rigid and dry surfaces, include: (1) stick, (2) spread, (3) disintegration or (4) rebound. Prediction of the exact mechanism involves accounting for the relative magnitude of the forces acting upon the droplet at impact, usually grouped in dimensionless numbers as in Table 8.1 There, the Mach number is not included, as it is associated with compressible effects, an issue not addressed here and for which the reader is referred to the various reviews on the subject, e.g., [1].

Surface boundary conditions (either geometrical or chemical) also alter the physics of the problem, but cannot be accurately included in any dimensionless parameter. Their effects are usually accounted by the topography of the surface and by the *wettability* of the surface to the liquid. The topography is characterized by the roughness amplitude (mean roughness, $R_a$ or mean peak-to valley roughness, $R_z$), by its fundamental wavelength (i.e., average distance between consecutive rough peaks) and shape of the asperities. The latter is difficult to quantify in practical surfaces, as their roughness profiles are stochastic, but it can be defined for custom made targets. After the pioneering work by Range and Feuillebois [2], who speculate on the relevance of these parameters, a renewed interest has recently been shown on the development of tailored surfaces in several practical situations (e.g., [3]), which thus confirm the relevant role of the geometrical relations between the topographical characteristics. However, it is essential to use a common terminology when referring to these parameters, to define all these quantities accurately, as well

A.L.N. Moreira (✉) and A.S. Moita
Department of Mechanical Engineering, Technical University of Lisbon – Instituto Superior Técnico, Lisbon, Portugal
e-mail: anamoita@dem.ist.utl.pt, moreira@dem.ist.utl.pt

**Table 8.1** Most relevant dimensionless numbers used in the analysis of droplet/(cold) surface interactions. $\rho$, $\mu$ and $\sigma_{lv}$ stand for liquid specific mass, dynamic viscosity and surface tension, respectively and g is the gravitational acceleration constant

| Dimensionless number | Definition | Relations |
|---|---|---|
| Weber number<br>Inertial forces/surface tension forces | $We = \frac{\rho U_0^2 D_0}{\sigma_{lv}}$ | |
| Reynolds number<br>Inertial forces/viscous forces | $Re = \frac{\rho U_0 D_0}{\mu}$ | |
| Capillary number<br>Viscous forces/surface tension forces | $Ca = \frac{\mu}{\sigma_{lv}} U_0$ | |
| Froude number<br>Inertial forces/gravitational forces | $Fr = \frac{U_0}{(gD_0)^{1/2}}$ | |
| Ohnesorge number<br>Viscous forces/surface tension forces | $Oh = \frac{\mu}{(\rho\sigma_{lv}D_0)^{1/2}}$ | $Oh = \frac{We^{1/2}}{Re}$ |
| Laplace number<br>Surface tension forces/momentum transport (dissipation) | $La = \frac{\rho\sigma_{lv}}{\mu^2} D_0$ | $La = \frac{Re^2}{We} = \frac{We}{Ca^2} = \frac{Re}{Ca} = Oh^{-2}$ |
| Bond number<br>Body (gravitational) forces/surface tension forces | $Bo = \frac{\rho g D_0^2}{\sigma_{lv}}$ | $Bo = \frac{We}{Fr}$ |

as standards to determine $R_a$ and $R_z$ (e.g., [4]) to avoid misleading interpretation of the results reported by different authors.

*Wettability* is a thermodynamic property of the interface solid-liquid–vapor, defined by the equilibrium contact angle $\theta$, given by the Young's equation:

$$\sigma_{ly} \cos\theta + \sigma_{ls} = \sigma_{sy} \tag{8.1}$$

where $\sigma_{lv}$, $\sigma_{ls}$ and $\sigma_{sv}$ are the interfacial tensions at the boundaries of the system liquid-surface-vapor. For low wetting surfaces, the contact angle varies in the range $90° < \theta < 180°$, while for partial wetting surfaces it is smaller than 90°, $0° < \theta < 90°$. Values of the contact angle $\theta = 0°$ and $\theta = 180°$ correspond to complete wetting or non-wetting, respectively.

However, the contact angle measured on a real surface, $\theta_R$, does not obey to Young's equation as this applies only to theoretically smooth surfaces. In general, the extent of liquid penetration into the roughness grooves is unknown and two extreme situations may occur: (1) the liquid penetrates completely within the grooves – the so called homogeneous wetting or (2) the liquid does not penetrate into the roughness grooves so that air pockets are entrapped between the liquid and the surface, which alters viscous dissipation – heterogeneous wetting.

The homogeneous wetting regime is accurately described by the classical theory of Wenzel, which relates the measured angle, $\theta_R = \theta_w$ with the Young angle, $\theta_Y$:

$$\cos\theta_w = r_f \cos\theta_Y \tag{8.2}$$

where $r_f$ is a roughness factor representing the ratio of the true wetted area to the correspondent apparent area. The heterogeneous regime is described by the

equation of Cassie and Baxter, where an apparent contact angle, $\theta_R = \theta_{CB}$ is defined as

$$\cos\theta_{CB} = -1 + f_w(r_f \cos\theta_Y + 1) \tag{8.3}$$

where $f_w$ is the fraction of the projected area of the solid surface that is wetted by the liquid. It is worth noting that the equation of Wenzel is a particular case of that of Cassie and Baxter for homogeneous wetting ($f_w = 1$). Transition between the homogeneous and the heterogeneous wetting regimes is not clear, though it is known to depend on surface chemistry and roughness, e.g., [5]. However, the equilibrium contact angle does not accurately represent the dynamic effects of the surface on droplet spread upon impact, and the dynamic contact angle is found to be more appropriate (e.g., [6]), though it has not been possible to obtain functional relations yet (e.g., [2]).

Regarding the outcomes of the impact, the spreading mechanism and their governing parameters are extensively described in the literature. This phenomenon is characterized by four stages, namely the *kinematic phase*, the *spreading phase*, the *recoiling phase* and the *equilibrium phase* (see [6], for the characterization of each phase). Inertial forces dominate the initial kinematic phase where the diameter of the spreading lamella increases with the square root of time

$$d(t) = CD_0\tau^{1/2} \tag{8.4}$$

where $\tau = t/(D_0/U_0)$). The spreading phase follows right after and is where the lamella expands up to its maximum diameter. Most approaches reported in the literature to describe this phase derive expressions for the maximum diameter and the time taken to reach it from the application of the conservation principles to the spreading lamella. Neglecting variations of the potential energy, the energy conservation principle gives:

$$E_{Ki} + E_{Si} = E_{Kf} + E_{Sf} + E_{diss} \tag{8.5}$$

where $E_K$ and $E_S$ refer to the kinetic and surface energy, respectively; $E_{diss}$ refers to the energy dissipated by viscous effects; subscripts $i$ and $f$ stand for the initial and final states, respectively. The initial kinetic energy is computed as:

$$E_{Ki} = (1/2)\rho U_0^2 Vol = (1/2\rho U_0^2)(1/6\pi D_0^3) \tag{8.6}$$

and the initial surface energy is computed considering the droplet spherical before impact:

$$E_{Si} = \int_0^{Vol} \Delta p dVol = 4\sigma_{lv}\pi R_0^2 = \sigma_{lv}\pi D_0^2 \tag{8.7}$$

The final state *f* is usually taken at the position where the diameter of the lamella is maximum, where $E_{\mathrm{diss}}$ and $E_{\mathrm{Sf}}$ can be easily determined. Major differences between the various existing models lay in the assumptions regarding the shape of the lamella, the estimation of $E_{\mathrm{Kf}}$ and $E_{\mathrm{diss}}$ and the way to account for *wettability* effects. Regarding the shape of the lamella, most models consider it as a cylindrical disk with instantaneous diameter $d(t)$ and height $h(t)$, so that relations between $d(t)$ and $D_0$ can be easily determined by mass conservation laws. Only recent models, e.g., [7] assume a more complex shape, in which the lamella is a thin film bounded by a thicker rim. Also, most of these models consider $E_{\mathrm{Kf}} = 0$ at maximum spread, which is not entirely correct, although it leads to good agreement with the experiments, probably because most are validated for impacts at small or moderate velocities. Again, few exceptions have been observed in recent works such as in Roisman et al. [7]. Though the energy dissipated, $E_{\mathrm{diss}}$ is also disregarded by some authors, it can be computed as:

$$E_{\mathrm{diss}} = \int_0^{t_2} \int_{Vol} \phi dVol dt \approx \phi Vol t_2 \tag{8.8}$$

where $\phi = \mu\left(\partial U_i/\partial x_j + \partial U_j/\partial x_i\right)\partial U_i/\partial x_j$ is the dissipation function and $t_2$ is a known time period after impact, for which the effect of viscous dissipation is expected to be relevant. The viscous dissipation function is subsequently scaled based on different assumptions. For instance, Pasandideh-Fard et al. [8] scale it with the impact velocity and with the boundary layer thickness, $\delta$. According to this, $\phi \approx \mu(U_0/\delta)^2$, for the boundary layer thickness estimated as in White [9], $\delta = 2D_0/(Re)^{1/2}$.

Further differences are found in the way the models account for *wettability* effects. These effects can be explicitly accounted in the spreading diameter by introducing the contact angle in the term of the surface energy of the spreading droplet, $E_{\mathrm{Sf}}$ as (e.g., [8]),$E_{\mathrm{Sf}} = (1/4)\pi d_{\max}^2 \sigma_{\mathrm{lv}}(1 - \cos\theta)$, where some authors use the equilibrium angle $\theta$, while others, particularly in more recent work, rather use the dynamic contact angle.

The *recoiling phase* occurs for partial wetting systems, while for complete wetting systems the lamella continues to spread over a long period after impact, clearly dominated by capillary forces, governed by the power law $d(t)/(D_0) = Ct^{1/10}$, as early proposed by Tanner [6].

## *Disintegration Mechanisms*

Contrary to spreading, the disintegration mechanisms are not so well documented in the literature. Several disintegration mechanisms can be identified: (a) prompt splash, (b) corona splash, (c) receding break-up (d) partial rebound, (e) finger break-up [10, 11].

The prompt splash is the mechanism usually addressed in the criteria for the spread/disintegration limits. The roughness amplitude, usually quantified by the mean roughness $R_a$, promotes the occurrence of such phenomenon at two different scales. Small roughness amplitudes ($R_a/R_0 < 3.4E - 4$) destabilize the lamella, while large roughness amplitudes ($R_a/R_0 > 2.5E - 3$) govern the disintegration mechanism [11]. Prompt splash takes place within the early instants after impact, being dominated by inertial forces. *Wettability* effects are observed only in extreme opposite situations: in low wetting systems ($\theta > 90°$), receding break-up and partial rebound are more likely to occur, while in complete wetting systems, ($\theta \approx 0°$), such as those formed by fuel droplets onto smooth surfaces, disintegration occurs after the formation of a crown (e.g., [10–12]), which destabilizes, disrupts into jets and further break up into secondary droplets. Despite some authors (e.g., [13]) state that the crown is induced by a kinematic discontinuity of the flow as proposed by Yarin and Weiss [14] for wetted surfaces, experimental studies show that such models do not predict accurately the growth rate of the crown (e.g., [11, 12]).

The development of the crown can be described as in Cossali et al. [14]. Referring to Fig. 8.1, crown diameters grow according to a power law:

$$\frac{D_c}{D_0} = C.(\tau - \tau_0)^n \tag{8.9}$$

where $0.41 < n < 0.45$ and $C$ is weakly dependent on liquid properties. This is in agreement with the theory proposed by Yarin and Weiss [15]. However, crown height and angle (and consequently the ejection angle of the secondary droplets) cannot be accurately described by this theory, since they are known to strongly depend on viscosity and aerodynamic forces. An alternative theory considers that the crown formation is driven by aerodynamic forces, according to the process described in Moita and Moreira [11] and Xu et al. [12]. This should be accounted in future models which consider the physical mechanisms of crown formation as performed, for instance, by Han et al. [16].

From the aforementioned, it is clear that the mechanisms of droplet disintegration depend in a complex way on the combination of the diverse conditions (e.g., droplet size, velocity and impact angle, surface topography and surface forces). The results of the systematic investigations reported by Rioboo et al. [10] and Moita and Moreira [11] are summarized in Table 8.2, where the arrows indicate the direction of change necessary to promote the occurrence of a particular mechanism. Dashed

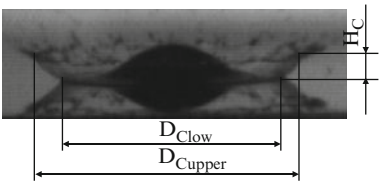


**Fig. 8.1** Crown morphology: $H_C$ crown height, $D_{Clow}$ crown lower diameter, $D_{Cupper}$ crown upper diameter

**Table 8.2** Effect of the various parameters to promote each disintegration mechanism: summary of the results reported by Rioboo et al. [10] and by Moita and Moreira [11] t2.1

| Increase of | Prompt splash | Corona splash | Receding break-up | Finger break-up | Partial rebound | t2.2 |
|---|---|---|---|---|---|---|
| $U_0$ | ↑ | ↑ | ↑ | ↑ | ↑ | t2.3 |
| $D_0$ | ↑ | | | | | t2.4 |
| $\sigma$ | ↓ | ↓ | ↑ | | ↑ | t2.5 |
| $\mu$ | ↓ | ↓ | ↓ | ↓ | | t2.6 |
| $R_a$ | ↑ | ↓ | | ↑ | ↓ | t2.7 |
| $\lambda_R$ | ↓ | ↓ | | | | t2.8 |
| $\theta$ | | ↓ | ↑ | ↓ | ↑ | t2.9 |

arrows indicate the additional contributions from the work which has been developed by Moita and Moreira [11]. 162 163

## *Secondary Atomization* 164

Besides, it is necessary to be able to predict which regime occurs at droplet impact. Threshold criteria are then defined which establish the boundaries between the four basic outcomes (stick, spread, rebound and disintegration). Particular emphasis is given here to the transition from spread to disintegration, due to its relevance to model the secondary spray generated at spray impact (e.g., [17]). Most criteria make use of the Weber number (e.g., [18]). However, care must be taken to assure that viscous effects are negligible (e.g., [2]), otherwise the Weber number alone does not describe the phenomenon. Prompt splash is then predicted to occur when inertial forces overcome capillary effects, i.e., when: 165 166 167 168 169 170 171 172 173

$$\rho U_0^2 > \frac{\sigma_{lv} h_L}{D_0^2} \tag{8.10}$$

where $h_L \sim (\nu D_0/U_0)^{1/2} = D_0 Re^{-1/2}$ is the thickness of the lamella (e.g., [15, 19]). If this relation is rewritten in terms of the dimensionless groups in Table 8.1, a "splashing parameter" is defined as 174 175 176

$$K_c = AOh^a We^b \tag{8.11}$$

This parameter, introduced by Stow and Hadfield [20] and later confirmed by Mundo et al. [21], is currently used in most correlations reported to predict the onset of splash. Although some of those correlations consider the effect of roughness amplitude (e.g., [20]), they still do not account for the complex mechanisms arising from the influence of other topographical parameters (e.g., [10–22]). This is the main reason for the discrepancies observed when the various criteria are compared and fitted to a diversity of experimental results. It is, therefore, unlikely that a unique criterion can accurately describe disintegration induced by any mechanism. 177 178 179 180 181 182 183 184

Given that impacting droplets may disintegrate by diverse mechanisms, secondary droplets are thus generated with dissimilar characteristics. Research efforts have also been put on the development of empirical sub-models to predict the size, velocity and number of secondary droplets. There are relatively few models valid for impacts onto dry surfaces. This must be taken into account, since major limitations to the use of these sub-models lies in the inaccurate consideration of the disintegration limits and in disregarding the boundary conditions for which they were validated.

## The Presence of a Liquid Film

The presence of a liquid film over the surface alters the boundary conditions, as the impact event now involves liquid/liquid interactions, though surface characteristics may still be important, depending on the thickness of the film. Based on the dimensionless roughness, $R_{ND} = R_a/D_0$ and on the dimensionless film thickness $\delta = h_f/D_0$ one may classify the impacts [23] as follows:

- Very thin film ($L_R/D_0 < \delta_f < 3R_{ND}^{0.16}$): droplet behavior at impact depends on surface topography. (In the absence of any other parameters besides $R_a$, Tropea and Marengo [23] define a "length scale of roughness"-$L_R$).
- Thin film ($3R_{ND}^{0.16} < \delta_f < 1.5$): the dependence of droplet behavior on surface topography becomes weaker.
- Thick film ($1.5 < \delta_f < 4$): droplet impact no longer depends on surface topography, but only on the film thickness.
- Deep pool ($\delta_f > 4$): droplet impact does not depend either on surface topography or on film thickness.

Here we focus on the impacts onto films with $\delta < 2$ since this condition is often satisfied in most practical spray applications. Similarly to droplet impingement on dry targets, diverse outcomes may occur: deposition and coalescence, bounce, formation of a crater, corona splash or uprising of a central jet. Most studies reported in the literature consider corona splash and focus on three issues: (1) characterization of crown morphology, (2) establishment of threshold criteria for disintegration and (3) characterization of secondary atomization.

### *Morphological Characterization*

The morphology of the crown is described with the temporal evolution of its diameter and height, as for impacts onto dry surfaces. Empirical laws for the diameter, valid for normalized film thickness $\delta \leq 1.13$ have been proposed (e.g., [14, 15]), which are similar to (8.9) but where $n = 0.5$ and the constant $C$ now depends on impact conditions:

$$C = 2.\left(\frac{2}{3}\right)^{0.25} U_0^{0.5} \cdot (D_0 h_0)^{-0.25} f^{-0.375} \tag{8.12}$$

where $f$ is the impact frequency, which for single droplets is taken as $D_0/U_0$.

The crown height is described by diverse expressions, depending on the relevant physical parameters of the phenomena. When the impact is governed by inertial forces and either viscous or compressibility effects are considered, after droplet impact, a kinematic discontinuity appears in the velocity distribution, due to the presence of the free surface of the pre-existing film. The liquid from the central spot spreads and forces the outward quiescent liquid, which is propelled upward and forms the crown. The formulation proposed by Roisman et al. [19] is found to be the most appropriate to describe crown formation and its evolution in the starting phase. At later stages, the discontinuity propagates towards the thicker section of the film and detaches part of it and propels it into the crown. In this case, the shape of the crown rim, $Y = Y(x, t)$, is governed by the eikonal equation which is useful to describe the cusp formation:

$$\frac{\partial Y}{\partial t} = V_{\text{rim}} \left[1 + \left(\frac{\partial Y}{\partial x}\right)^2\right]^{1/2} \tag{8.13}$$

here $V_{\text{rim}}$ is the velocity of the free rim propagating over the crown wall, $Y$ is the coordinate along the crown surface and $x$ is the circumferential coordinate over the crown. Although of relative minor importance for impacts onto wetted targets, the surface topography may not negligible, although studies on its effects are quite sparse (e.g., [13]). These studies mainly report that increasing roughness amplitude promotes crown disturbances and further disintegration, which is understandable, based on the discussion for impacts onto dry surfaces.

## *Impact Regimes and Secondary Atomization*

As for the impacts onto dry surfaces, the most straightforward and usual approach is to distinguish between the four basic impact outcomes (stick, spread, rebound and disintegration) by establishing straight boundaries. The boundaries stick/spread, spread/rebound, are often defined by threshold values of the Weber number. For instance, the limit for stick/spread is often set at $We < 5$, while the limit for spread/rebound is usually given as $We < 10$ (e.g., [16, 17]). Concerning the limits for spread/disintegration the force balance in (8.10) is still valid here, although the boundary conditions are different. In line with this, the group $K_c = Oh^{-0.4}We$ is still of major importance, but then, the empirical correlations have to be adjusted by including other parameters such as the film thickness. Hence, correlations for the spread/disintegration limits are of type: $K_{c,\text{wet}} = f(K_c, \delta)$ (e.g., [15, 22]).

Secondary droplet characteristics can also be predicted from semi-empirical models. This subject is not addressed here but the reader is referred to the various reviews (e.g., [24]) which analyze the models proposed for impacts onto wetted and cold surfaces (e.g., [16, 17, 19]).

## The Additional Effects of Heat Transfer

Depending on the surface temperature, diverse heat transfer mechanisms may develop when a droplet impacts onto a heated surface, which can be described by the classical boiling curve of a droplet gently deposited on a heated surface (see Fig. 8.2: (1) film evaporation ($T_W \leq T_{sat}$, where $T_{sat}$ is the liquid saturation temperature), (2) bubble boiling ($T_{sat} \leq T_w \leq T_{Nukiyama}$), (3) transition ($T_{Nukiyama} \leq T_W \leq T_{Leidenfrost}$) and (4) film boiling ($T_W \geq T_{Leidenfrost}$).

For the case of an impacting droplet, the critical temperatures establishing the transition between these regimes, particularly the Leidenfrost temperature, depend on the impact conditions, as well as on the properties of the system liquid-surface-vapor. An extensive review on the Leidenfrost temperature and their influencing parameters is presented by Bernardin and Mudawar [25, 26]. Also, though the heat transfer regimes for an impacting droplet ($U_0 \neq 0$) are qualitatively similar to those for a sessile droplet, they are quantitatively different. For example, while for a sessile droplet the film boiling regime is characterized by the formation of a vapor layer, which precludes the contact between the droplet and the surface, the dynamic analog is the reflection (rebound) of the impinging droplet from the surface.

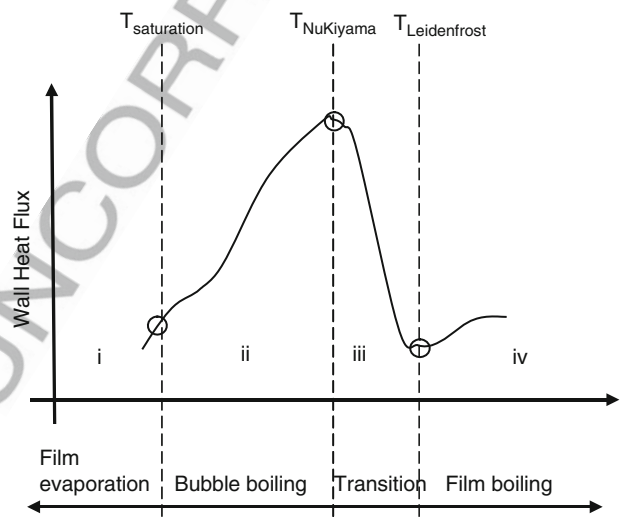


**Fig. 8.2** Heat transfer regimes, as described by the classical boiling theory

However, in the latter case, the temperature at which there is in fact no contact between the droplet and the surface, (the so called dynamic Leidenfrost temperature) is very high and it depends on the Weber impact number (e.g., [27]). To avoid misleading, many authors identify the film boiling regime based on a morphological analysis and consider that the droplet falls within the film boiling regime at the so called reflection or pure rebound temperature [17], which is slightly below the dynamic $T_{\text{Leidenfrost}}$.

## *Morphological Characterization*

Figure 8.3 depicts the various outcomes of a droplet impacting with velocity $U_0$ onto a smooth surface at increased surface temperatures $T_w$. The images evidence that the relative importance of the effects governing droplet break-up depends on the heat transfer regime.

Within the bubble boiling regime, the secondary atomization occurs within a time scale long enough to allow phase transition of the liquid. Hence, the disintegration occurs at later stages of spreading as the vapor pressure forces disrupt the thin surface area of the lamella. Consistently, the secondary droplets are mainly ejected upwards and droplet morphology is not much influenced by the impact velocity.

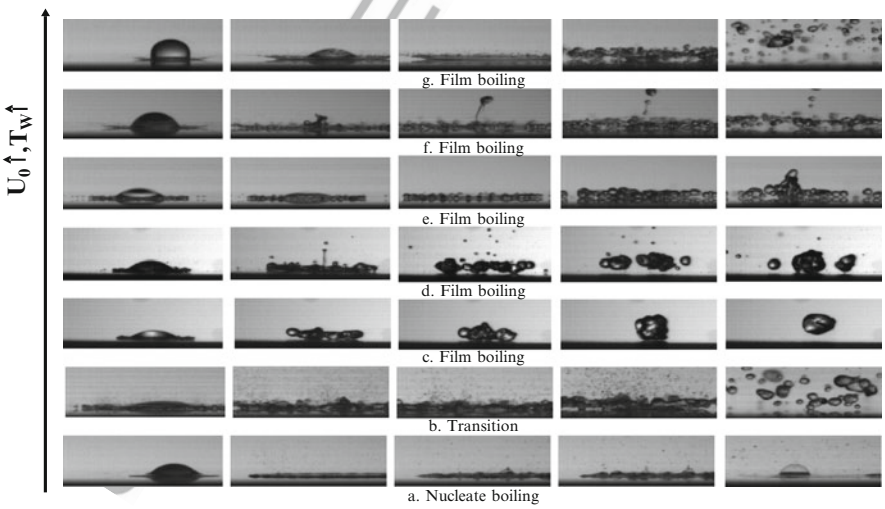


**Fig. 8.3** Morphology of an ethanol droplet ($D_0 = 2.4$ mm) impacting onto a smooth stainless steel surface ($R_a = 0.311$ μm, $R_z = 2.32$ μm) at different surface temperatures and impact velocities: (a) $T_w = 115°C$, $U_0 = 2.5$ ms$^{-1}$, (b) $T_w = 150°C$, $U_0 = 2.5$ ms$^{-1}$, (c) $T_w = 300°C$, $U_0 = 0.5$ ms$^{-1}$, (d) $T_w = 300°C$, $U_0 = 0.8$ ms$^{-1}$, (e) $T_w = 300°C$, $U_0 = 1.3$ ms$^{-1}$, (f) $T_w = 300°C$, $U_0 = 2.5$ ms$^{-1}$ (formation of the central jet), (g) $T_w = 300°C$, $U_0 = 2.5$ms$^{-1}$ (crown formation)

As the droplet impacts the surface within the film boiling regime, the lamella disintegrates almost immediately after impact, mainly in the radial direction, at the edge of the lamella as for prompt splash onto cold surfaces. Then, a number of large droplets are generated after the levitation of the lamella. The inertial forces dominate the disintegration mechanism within this short time period and droplet morphology is very sensitive to impact velocity. Viscous dissipation is of minor importance but, instead, the vapor film is responsible for the dissipation of kinetic energy.

## Impact Regimes and Secondary Atomization

When the impact occurs onto a heated surface, besides the disintegration mechanisms described for impacts onto cold surfaces, disintegration may also occur by thermal induced mechanisms.

Rebound (with or without disintegration), prompt disintegration, (at low $U_0$) and corona splash are the mechanisms observed at the film boiling regime. Few authors proposed a global representation to explain all possible impact outcomes within the various heat transfer regimes as a function of the Weber number and of the surface temperature (e.g., [17]). Although this approach provides a good qualitative interpretation, the background physics is quite complex. Therefore, most authors rather prefer to analyze the disintegration regimes and the secondary droplet characteristics within each regime, separately (e.g., [28]). Thermal-induced disintegration has been addressed in recent researches (e.g., [29–31]) from which correlations can be devised to predict secondary droplet characteristics within the various boiling regimes. Here the emphasis is given to droplet size.

Within the bubble boiling regime, thermal induced disintegration occurs when the vapor pressure unbalances the equilibrium between surface tension, viscous forces and inertial forces. The nature of this mechanism is different from those observed onto cold surfaces, as it is triggered by combined effects induced by the liquid surface tension and the latent heat of evaporation, $h_{fg}$, and the analysis requires the use of dimensionless groups complementary to those in Table 8.1. The most important is the Jakob number, defined as $Ja = C_p(T_W - T_{sat})/h_{fg}$ where $C_p$ is the specific heat of the liquid.

The Jakob number is relevant within the transition regime given the violent boiling occurring within the early instants after impact, before the lamella levitates. On the other hand, there is an evident relation of droplet morphology with the Weber number, as shown in Fig. 8.3.

Within the film boiling regime, the disintegration is clearly dominated by inertial effects and the size of secondary droplets correlate with the thickness of the lamella as defined for the impact onto a dry wall, $h_L \sim (\nu D_0/U_0)^{1/2} = D_0 \mathrm{Re}^{-1/2}$ (e.g., [19]). The following relation is suggested by Moita and Moreira [32] to predict the size of secondary droplets:

$$\frac{\mathrm{SMD}}{D_0} = f(We, Re) \sim A_2 We_N^{-0.6} Re^{-0.23} \tag{8.14}$$

It is worth mentioning that any of the proposed relations accounts with surface topography (the relation suggested by Moita and Moreira (2009) [32] is valid only for $R_a/D_0 < 2E - 3$). The role of surface topography is far more complex than promoting droplet disintegration, especially when dealing with heated targets as it significantly alters the fluid dynamic and thermal behavior of the impinging droplets. Tailored surfaces have quite different wetting behaviors and may be used to enhance liquid/surface contact or, instead to produce hydrophobic behaviors. Distinct results can be obtained in terms of secondary atomization and thermal behavior, depending, once again on the heat transfer regime which is being considered. In line with this, surface topography may even degrade the thermal behavior of the droplet. Optimization of the topographical parameters, based on the relations between $R_a/\lambda_R$, is therefore a compromising solution of endorsing liquid–solid contact without promoting an excessively intense thermal induced atomization.

## Final Remarks

Droplet/wall interactions were described for impacts onto non-heated dry surfaces to which further complexities were gradually added considering, first the presence of a liquid film and then surface heating. Diverse outcomes develop from droplet impact, depending on impact conditions and surface boundary conditions (e.g., *wettability* and topography). The onset of disintegration depends on the competition between inertial and capillary effects and is shown to scale with a splashing parameter $K_c = AOh^a We^b$. A variety of disintegration mechanisms have been identified, within very dissimilar time scales, so that the relative importance of the governing parameters is different. Therefore, though it is possible to identify general trends, different relations must be considered to predict the secondary droplet characteristics for each mechanism.

## References

1. M. Lesser: The impact of a compressible liquid, In Drop-surface interactions, M. Rein (Ed.), Springer Wien, New York, p. 39 (2002).
2. K. Range, F. Feuillebois: Influence of surface roughness on liquid drop impact, J. Col. Int. Sci., 203, 16–30 (1998).
3. D. Sivakumar: Spreading behaviour of an impacting drop on a structured rough surface, Phys. Fluids, 17, 100608 (2005).
4. T. Thomas (Ed.): Rough surfaces, Longman Group Limited (1982).
5. C. W. Extrand: Criteria for ultralyphobic surfaces, Langmuir, 20, 5013–5018 (2004).

6. R. Rioboo, M. Marengo, C. Tropea: Time evolution of liquid drop impact onto solid, dry surfaces, Exp. Fluids, 33(1), 112–124 (2002).
7. I. V. Roisman, R. Rioboo, C. Tropea: Normal impact of a liquid drop on a dry surface: model for spreading and receding, Proc. R. Soc. Lond. Ser. A, 458, 1411–1430 (2002).
8. M. Pasandideh-Fard, Y. M. Qiao, S. Chandra, J. Mostaghimi: Capillary effects during droplet impact on a solid surface, Phys. Fluids, 8(3), 650–658 (1006).
9. M. White: Viscous fluid flow, 2nd edn., McGraw-Hill, New-York (1991).
10. R. Rioboo, C. Tropea, M. Marengo: Outcome from a drop impact on solid surfaces, Atom. Sprays, 11, 155–165 (2001).
11. S. Moita, A. L. N. Moreira: Drop impacts onto cold and heated rigid surfaces: Morphological comparisons, disintegration limits and secondary atomization, Int. J. Heat Fluid Flow, 28(4), 735–752(2007).
12. L. Xu, W. W. Zahang, S. R. Nagel: Drop splashing onto a dry smooth surface, Phys. Rev. Lett., 94, 184505 (2005).
13. L. Randy, G. Vander Wall, G. M. Berger, S. D. Mozes: The combined influence of a rough surface and thin fluid film upon the splashing threshold and splash dynamics of a droplet impacting onto them, Exp. Fluids, 40, 23–32 (2006).
14. G. E. Cossali, M. Marengo, A. Coghe, S. Zhdanov: The role of time in single droplet splash on thin film, Exp. Fluids, 36(6), 888–900 (2004).
15. L. Yarin, D. A. Weiss: Impact of drops on solid surfaces: Self-similar capillary waves and splashing as a new type of kinematic discontinuity, J. Fluid Mech., 283, 141–173 (1995).
16. Z. Han, Z. Xu, N. Trigui: Spray/wall interaction models for multidimensional engine simulation, Int. J. Eng. Res., 1(1), 127–146 (2000).
17. C. X. Bai, A. D. Gosman: Development of a methodology for spray impingement simulation, SAE Paper 950283 (1995).
18. M. Gavaises, A. Theodorakakos, G. Bergeles: Modeling wall impaction of diesel sprays, Int. J. Heat Fluid Flow, 17(2), 130–138 (1996).
19. V. Roisman, K. Horvat, C. Tropea: Spray impact: Rim transverse instability initiating fingering and splash: Description of a secondary spray, Phys. Fluids, 18, 102104 (2006).
20. D. Stow, M. G. Hadfield: An experimental investigation of fluid flow resulting from the impact of a water drop with an unyielding dry surface, Proc. R. Soc. Lond. Ser. A, 373, 419–441 (1981).
21. C. Mundo, C. Tropea, M. Sommerfeld: On the modelling of liquid sprays impinging on surfaces, Atom. Sprays, 8, 625–652 (1998).
22. G. E. Cossali, A. Coghe, M. Marengo: The impact of a single drop on a wetted solid surface, Exp. Fluids, 22, 463–472 (1997).
23. Tropea, M. Marengo: The impact of drops on walls and films, Multiphase Sci. Tech., 11(1), 19–36 (1999).
24. S. Y. Lee, S. U. Ryu: Recent progress of spray-wall interaction research, J. Mech. Sci. Tech., 20(8), 1101–1117 (2006).
25. J. D. Bernardin, I. Mudawar: The Leidenfrost point: Experimental study and assessment of existing models, Trans. ASME, 121, 894–903 (1999).
26. J. D. Bernardin, I. Mudawar: A Leidenfrost point model for impinging droplets and sprays, ASME J. Heat Transfer, 126, 272–278 (2004).
27. H. Xie, Z. Zhou: A model for droplet evaporation near Leidenfrost point, Int. J. Heat Mass Transfer, 50, 5238–5333 (2007).
28. S. W. Akhtar, A. J. Yule: Droplet impaction on a heated surface at high Weber numbers, In: Proceedings of the ILASS-Europe 2001, Zurich (2001).
29. J. D. Naber, P. Farrel: Hydrodynamics of droplet impingement on a heated surface, SAE Paper 930919 (1993).
30. G. E. Cossali, M. Marengo, M. Santini: Secondary atomization produced by single drop vertical impacts onto heated surfaces, Exp. Thermal Fluid Sci., 29, 937–946 (2005).

31. A. L. N. Moreira, A. S. Moita, E. Cossali, M. Marengo, M. Santini: Secondary atomization of water and isooctane drops impinging on tilted heated surfaces, Exp. Fluids, 43, 297–313 (2007).
32. S. Moita, A. L. N. Moreira: Development of correlations to predict the secondary droplet size of impacting droplets onto heated surfaces, Exp. Fluids, 47, 755–768 (2009).

# Splashing and Fragmentation of Droplets Landing on a Solid Surface

Sanjeev Chandra

## Introduction

Driving through rain you can observe water drops hitting the windscreen and splashing, fragmenting into smaller droplets. The sight is fascinating, but the moment too fleeting to observe the details of how a liquid drop splashes. It was not until Worthington [1] built an ingenious apparatus that used the spark from an electric capacitor discharge to illuminate impacting droplets and freeze their motion long enough to take photographs that the details of fluid motion during droplet impact became visible. Decades later, when electronic flash became widely available, Edgerton [2] took pictures of splashing milk droplets that have since been widely reproduced so that the crown-like shape of a splashing droplet is instantly recognizable.

Figure 8.4 shows photographs of successive stages during the impact of a 2.7 mm diameter molten tin droplet impacting with a velocity of 4 m/s on a stainless steel plate [3]. Both drop and plate are at a temperature of 240°C, above the melting point of tin (232°C) so that impact is isothermal. The drop, initially spherical, begins to deform very rapidly upon contact and a thin liquid sheet begins to spread radially under it. The liquid–solid contact line edge of this sheet becomes unstable as it advances and a periodic disturbance is visible around it. Once the droplet reaches its maximum extension surface tension, which is very strong in molten metals, begins to pull it back. Because the molten metal does not wet the steel substrate well the fingers grow longer and break-up into smaller satellite droplets. The remaining liquid bounces off the substrate.

Since early photographic studies first revealed the complex dynamics of droplet impact, splashing has been studied intensively. It is fascinating from the view of fundamental fluid mechanics since many of the phenomena involved, such as the rapid deformation of free liquid surfaces, the motion of liquid–solid contact lines,

S. Chandra
Department of Mechanical and Industrial Engineering, University of Toronto, Toronto, Ontario, Canada
e-mail: Chandra@mie.utoronto.ca

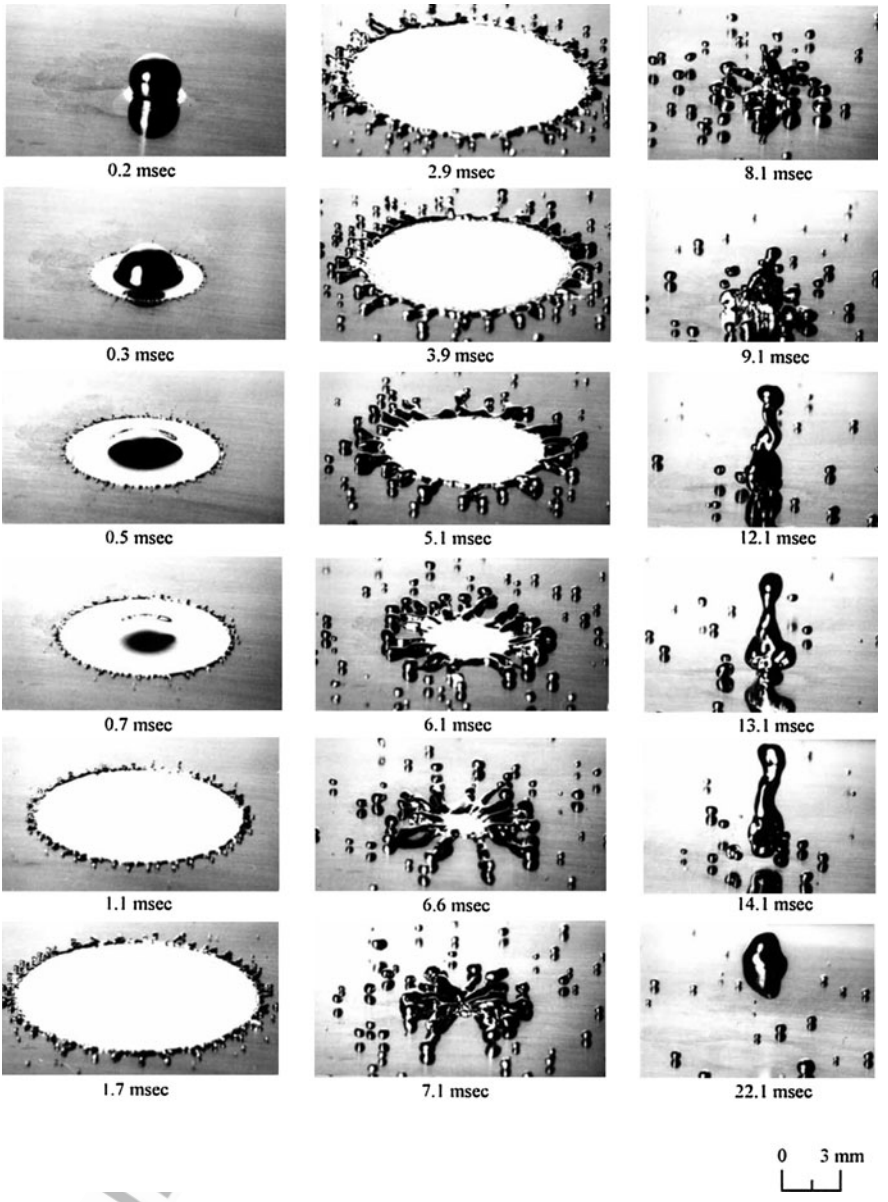


**Fig. 8.4** Splashing of a 2.7 mm diameter molten tin droplet during impact with velocity 4 m/s on a stainless steel surface at temperature 240°C. The droplet and substrate are both above the melting point of tin (232°C) so there is no freezing [3]

and the onset of fluid instabilities are not still well understood. There are, in addition, a host of industrial technologies where droplet splashing is important. In spray coating and painting, pesticides application or spray quenching of hot

surfaces it is important to prevent droplet fragmentations since satellite droplets bounce off the surface, reducing the sprayed material that stays on the surface [4]. The quality of pictures printed using an ink-jet technique depend on the accuracy with which droplets are placed on paper: splashing results in random deposition of ink and degrades the image [5]. Splashing may be helpful in preventing accumulation of water on surfaces, which can freeze and lead to ice accretion on aircraft and buildings [6]. The shape of splashes can provide information in forensic studies of blood splatter, from which the size and velocity of droplets can be deduced [7]. As a consequence of this interest a large number of studies of droplet splashing have been carried out and the early literature has been reviewed in detail by Rein [8] and Yarin [9].

When a droplet collides with a surface, there are three phases involved: liquid (the droplet), solid (the substrate) and gas (the surrounding atmosphere). A droplet is described by two impact parameters, diameter ($D_d$) and impact velocity ($V_d$), and three physical properties: liquid density ($\rho_l$), viscosity ($\mu$), and liquid–gas surface tension ($\gamma_{lg}$). Combining these into non-dimensional groupings we obtain the Reynolds number ($Re = \rho_l V_d D_d/\mu$) and Weber number ($We = \rho_l V_d{}^2 D_d/\gamma_{lg}$). The Weber number is a ratio comparing inertial forces, which drive splashing, to surface forces that hold the droplet intact. Similarly, the Reynolds number is a ratio of the droplet inertia to viscous forces that damp out motion. Droplets are more likely to splash when $Re$ and $We$ are large. However these two parameters alone do not provide adequate information to predict if splashing will always occur since they do not describe the effect of the substrate and surrounding gas.

The topology of the substrate affects fluid flow and this is typically described by specifying the average surface roughness ($R_a$). Stow and Hadfield [10] studied the effects of surface roughness on spreading and splashing of water droplets and established that splashing was promoted by increasing drop diameter ($D_d$), impact velocity ($V_d$), and surface roughness ($R_a$). They combined the Reynolds and Weber numbers to define a dimensionless "splash factor" equal to $ReWe^2$ and droplet splashing was observed if this parameter exceeded a critical value, whose value depended on surface roughness. Subsequent studies developed empirical correlation between the splash factor and surface roughness [11–14] but these have been of limited use in predicting whether splashing will occur in impacts that are not very close to the conditions for which experiments were conducted.

Droplet properties and surface roughness alone are not sufficient to account for splashing. Once liquid contacts the solid surface the total surface energy of the system is determined by the surface tension of liquid–solid ($\gamma_{ls}$), liquid–gas ($\gamma_{lg}$) and solid–gas ($\gamma_{sg}$) interfaces. Since $\gamma_{ls}$ and $\gamma_{sg}$ are usually not well known it is convenient to replace them with the equilibrium contact angle ($\theta$) using Young's equation:

$$\gamma_{lg} \cos\theta = \gamma_{sg} - \gamma_{ls}$$

The wettability of the surface, characterized by $\theta$, is therefore important in modelling droplet impact. Since the contact line is moving the dynamic advancing

($\theta_a$) and receding ($\theta_r$) contact angles also have to be considered, depending on whether the droplet edge is spreading outwards or retreating.

As the droplet approaches the substrate, the gas between them has to be expelled and its density and viscosity determine how rapidly this occurs [15, 16]. The gas film trapped at the liquid–solid interface forms a bubble [17]. Then as the edges of the droplet spread out they face resistance from the surrounding atmosphere that has to be pushed back. Xu, Zhang and Nagel [18] demonstrated that lowering the pressure of the surrounding atmosphere suppresses splashing. Figure 8.5 shows photographs of alcohol droplets landing on a smooth glass plate. At atmospheric pressure the droplet splashes, but when pressure is reduced no splashing is seen.

Some of the difficulty in predicting when splashing will occur can be attributed to uncertainties about surface wettability and the effect of the surrounding atmosphere. However, there is a certain ambiguity about the concept of "splashing" itself. Several different break-up modes are grouped under the same term, even though the mechanism of each may be quite different. Rioboo et al. [19] identified three different types of splashing, shown in Fig. 8.6 Immediately after impact, as the liquid sheet under the droplet spreads out, its edge becomes unstable and fingers around the edge begin to break off and form small droplets. This has been termed "prompt splash" and occurs when the edge of the lamella is still in contact with the

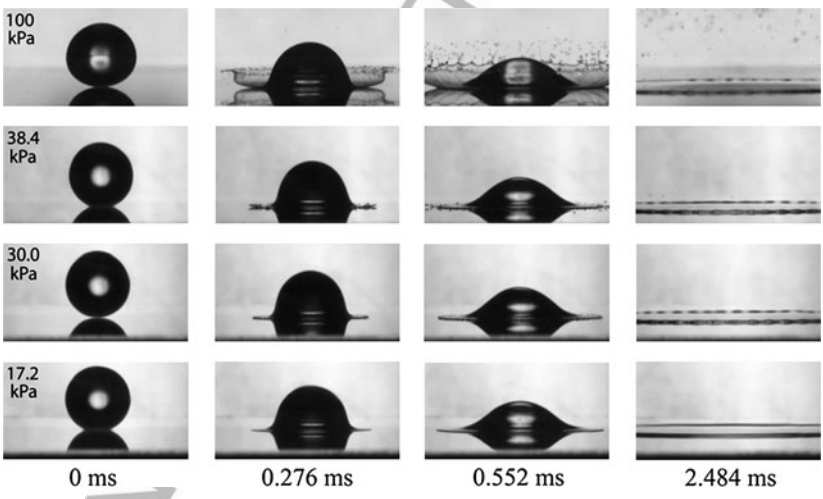


**Fig. 8.5** Photographs of a liquid drop hitting a smooth dry substrate. A 3.4 mm diameter alcohol drop hits a smooth glass substrate at impact velocity 3.74 m/s in the presence of different background pressures of air. Each row shows the drop at four times. The first frame shows the drop just as it is about to hit the substrate. The next three frames in each row show the evolution of the drop at 0.276, at 0.552, and at 2.484 ms after impact. In the top row, with the air at 100 kPa (atmospheric pressure), the drop splashes. In the second row, with the air just slightly above the threshold pressure, 38:4 kPa, the drop emits only a few droplets. In the third row, at a pressure of 30.0 kPa, no droplets are emitted and no splashing occurs. However, there is an undulation in the thickness of the rim. In the fourth row, taken at 17.2 kPa, there is no splashing and no apparent undulations in the rim of the drop [18]

surface. The second type of splashing has been termed "corona" splashing: the liquid lamella lifts off the surface, the edge becomes unstable so that fingers grow at regular spaced intervals and the tips of these break off in the crown-like shape characteristic of splashing drops. The third row in Fig 8.6. shows "receding break-up," in which the droplet remains intact until it has spread to its maximum extent and then, as surface tension forces pull it back, the fingers formed due to instabilities around its periphery grow longer and begin to breakup into smaller droplets.

Apart from these three mechanisms, there are two others that can cause break-up of impacting droplets. If a droplet impacts on a substrate that is cold enough to cause freezing, the solid layer formed at the liquid–substrate interface acts as a barrier. The spreading liquid hits the solid mass obstructing its path, jets upwards and disintegrates. This is known as freezing-induced splashing [20] and whether it occurs depends on the rate of heat transfer between the droplet and substrate, which is controlled by the substrate temperature, substrate thermal properties, and the thermal contact resistance at the liquid–solid interface.

There is yet one more mechanism that leads to droplet fragmentation, when impact velocities are very high so that the liquid film becomes very thin and air bubbles trapped under it break through. These punctures in the liquid grow larger and can eventually lead to complete disintegration of the droplet [21].

## Prompt Splashing

Prompt splashing is observed immediately after a droplet impacts on a surface and is promoted by increasing impact velocity, droplet diameter and surface roughness [19]. Immediately after impact a very thin liquid lamella emerges from below the droplet and expands radially outwards. The thickness of the liquid sheet, initially a few microns, increases as it spreads [22]. Initially, if the liquid thickness is small and its velocity high, if it hits any obstruction on the surface it is diverted upwards, becoming airborne [23]. The edge of the liquid film becomes unstable as it continues to rise up and disintegrate, releasing satellite droplets. Satellite droplets are shed continuously from the advancing contact line (see Fig. 8.6). Similarly, a

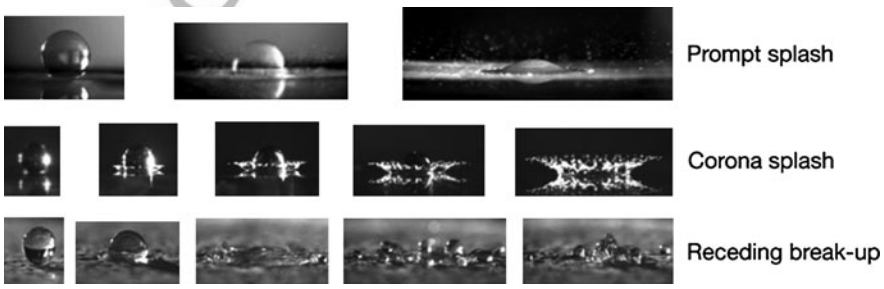


**Fig. 8.6** Different types of splashing during droplet impact [19]

droplet deposited inside a rectangular slot splashes when the spreading liquid hits the vertical walls of the slot and rises upwards [24].

A rough surface has a large number of surface asperities that act as obstacles, promoting prompt splashing [25]. If the surface has asperities that are significant in height, compared to the thickness of the liquid film the edges of the film become unstable and disintegrate releasing small satellite droplets. For splashing to occur, the liquid must have enough momentum so that it rises over the obstructions rather than being halted by them. Xu Barcos and Nagel [25] postulated that prompt splashing occurs if the average surface roughness $R_a$ is greater than $Ch$, where $h$ is the liquid lamella thickness and $C$ is a function of $Re$ and $We$. In their experiments they found that $h = 50$ μm and $R_a = 5$ μm, and concluded that $C \sim 0.1$.

Once prompt splashing occurs the liquid lamella thickness continues to increase as more liquid flows from the droplet into the spreading film, while its velocity diminishes [22]. Both of these factors combine to suppress edge instabilities and therefore prompt splashing is typically seen only briefly during droplet impact, during the earliest stages of collision. During experiments carried out at high impact velocities ~40 m/s) it becomes more difficult to differentiate between prompt splashes and corona splashes [21, 26] since the rapidly spreading liquid lamella quickly overruns the thin liquid ligaments that are formed during prompt splashing.

On artificially textured surfaces, where pillars are etched in a square array, splashing occurs along the diagonals, where the liquid meets more resistance, but not along the channels between pillars where it can flow easily [27]. Prompt splashing is sensitive to the spacing, height and arrangement of pillars [28].

## Corona Splashes

When a droplet spreads into a thin liquid film the surrounding gas pushes against it, creating an adverse pressure gradient that eventually lifts the edge of the liquid lamella off the surface. The edge of the liquid sheet becomes unstable so that undulations begin to form, grow into long fingers and then detach in the form of satellite droplets (see Fig. 8.5). Schroll et al. [29] numerically simulated the impact of a viscous liquid drop onto a smooth dry solid surface, including the effect of the surrounding air. The no-slip boundary condition at the wall produces a boundary layer inside the liquid. As the radial expansion slows the pressure gradient within the liquid sheet drops to zero and the boundary layer is not securely attached to the wall. An adverse pressure gradient, created by resistance from the surrounding airflow, can cause the boundary layer to separate from the wall so that the liquid layer rises up to form a corona. Much more prominent corona splashes are seen when a droplet lands on a thin liquid film since the surrounding quiescent liquid offers strong resistance to the spreading. The adverse pressure gradient creates a corona that breaks up [30, 31].

Many studies have been devoted to predicting when corona splashes will occur. Mundo, Sommerfeld, and Tropea [11] found that droplets splashed only if the so-

called "splash parameter" $K = We^{1/2}Re^{1/4}$ exceeds a critical value $K = 57.7$. Cossali, Coghe and Marengo [30] developed an empirical correlation between $K$, $R_a$ and the liquid lamella thickness $h$.

The nature of the instability that initiates formation of fingers around the edges of the spreading droplet has been the subject of much debate [9]. Allen [32] suggested that fingering is initiated by a Rayleigh-Taylor instability that occurs at the interface between liquid and surrounding gas when the lighter gas pushes the heavier liquid. Linear instability analysis predicts that the fastest growing disturbances at a planar liquid–gas interface will have a wavelength:

$$\lambda = 2\pi\sqrt{\frac{3\gamma_{lg}}{a(\rho_l - \rho_g)}}$$

where $a$ is the deceleration of the interface and $\rho_l$ and $\rho_g$ the densities of the liquid and surrounding gas respectively. Allen [32] estimated $a = V_d^2/(D_{max}/2)$, with $D_{max}$ the diameter of the droplet at its maximum extension, so that the number of fingers $N = \pi D_{max}/\lambda$. He demonstrated reasonable agreement between predictions and the number of fingers around ink blots formed by drops falling on a piece of paper. Bhola and Chandra [33] proposed that $a = V_d^2/D_d$, and using a simple energy balance model to calculate $D_{max}$, obtained:

$$N = \frac{\left(We^{1/2}Re^{1/4}\right)}{\left(4\sqrt{3}\right)} = \frac{K}{\left(4\sqrt{3}\right)}$$

Range and Feuillebois [34] studied splashing of droplets of water–glycerin and water–ink mixtures and found that the number of fingers was sensitive to the surface tension of the liquid, but not its viscosity. Kim, Feng and Chun [35] presented a Rayleigh-Taylor instability analysis of the liquid sheet emerging from under the drop, solving the potential flow equation. They neglected the effect of viscosity, arguing that formation of fingers is initiated immediately after droplet impact, when viscous forces are negligible. They solved the governing equations numerically, to obtain the fastest growing wavelength as a function of $We$. Since viscous effects were neglected, the solution was independent of $Re$. Mehdizadeh, Chandra, Mostaghimi [21] found an analytical solution to the equations governing the Rayleigh-Taylor instability and found that $N = 1.14\ We^{1/2}$ predicted reasonably the number of fingers formed around water droplets over a wide range of $We$. Fedorchenko and Chernov [36] claimed the initial radial liquid velocity equals the sonic velocity in the liquid therefore the liquid lamella experiences very high deceleration, sufficient to trigger the Rayleigh–Taylor instability. Pepper, Courbin and Stone [37] measured lamella deceleration as high as $10^3 g$.

The air film trapped under the impacting droplet plays an important role in creating instabilities. Xu, Zhang, Nagel [18] demonstrated that if the pressure in the atmosphere surrounding an impacting drop is reduced corona splashes are

suppressed. Prompt splashing, however, persists even in the absence of surrounding gas [25]. Thoroddsen and Sakakibara (1998) photographed water droplets landing on a glass plate, viewed from below during very early stages of impact and showed that the instability begins immediately at the first contact of the drop with the solid surface. The bottom of the droplet becomes flattened as the droplet approaches the surface due to the increase in pressure in the air gap between the liquid and solid surface. Thoroddsen and Sakakibara [38] proposed that fingering is initiated by a Rayleigh–Taylor instability of the annular ring of fluid that first touches the surface, which is then propagated over to the radially expanding sheet of liquid.

Yoon et al. [39] also emphasized the importance of the air trapped between the droplet and substrate. They pointed out that the Rayleigh-Taylor instability should continue to occur even if the density of the surrounding gas goes to zero, which contradicts the findings of Xu, Zhang and Nagel [18] that splashing disappeared when gas pressure was reduced. They proposed instead that fingering is initiated by a Kelvin-Helmholtz instability that occurs when the heavier liquid spreads over a thin gas film that is trapped between the droplet and substrate.

The dominant wavelength for a Kelvin-Helmhotz instability is [40]

$$\lambda = 2\pi\sqrt{\frac{3\sigma}{a\rho_g V_{diff}^2}}$$

where $V_{diff}$ is the velocity difference between the liquid and gas layers. In the limit that $\rho_g \to 0$ the instability is suppressed, which agrees with the observations of Xu, Zhang and Nagel [18]. Yoon et al. [40] have proposed that it is the Kelvin-Helmholtz, rather than the Rayleigh-Taylor, instability that leads to initiation of fingers around the edges of spreading drops.

When droplets impact on an elastic membrane splashing can be suppressed by reducing the tension of the substrate [37]. The flexible substrate absorbs some energy, but it also makes it easier for air to escape from below the droplet, which reduces splashing.

## Receding Breakup

Once a droplet has reached its maximum extension after impact, surface tension forces pull it edges back. If the liquid-solid contact angle is small, less than 90°, neighboring fingers along the edges of the spreading liquid sheet tend to merge with each other [38] and disappear. However, if the contact angle is large, as is the case with droplets of molten metal [3] or for impact on super-hydrophobic surfaces [41] the fingers stay well defined and grow longer as the liquid recedes. The cylindrical fingers become unstable and begin to break-up into become so long that they disintegrate (see Fig. 8.4).

## Freezing Induced Splashing

The presence of solid asperities on the substrate promotes splashing since it obstructs the flow of the spreading droplet. In the case that the droplet spreads on a substrate at a temperature lower than the freezing point of the liquid, it will begin to solidify. If heat transfer from the spreading droplet to the substrate is rapid, the rate of solidification in the droplet becomes sufficiently fast that its edges begin to freeze and form a solid ring, while liquid is still flowing radially outwards. If the droplet Weber number is low the solid layer will stop liquid motion and suppress splashing since the impacting liquid does not have enough momentum to jet over the solidified layer near the edges of droplets and splash [3]. If the Weber number is high the solid layer acts as a surface asperity that promotes splashing: the radially spreading liquid will hit the obstruction, become unstable, and break into satellite droplets.

Mehdizadeh et al. [21] built an apparatus in which molten tin droplets impinged on a steel plate mounted on the rim of a rotating flywheel, giving impact velocities of up to 40 m/s and $We \sim 10^3$. Photographs of splashing droplets were compared with predictions from computer simulations that showed that freezing around the edges of a spreading droplet obstructs liquid flow and causes splashing. Dhiman and Chandra [20] photographed impact of molten tin droplets on solid plates for a range of impact velocities (10–30 m/s), substrate temperature (25°C–200°C) and substrate materials (stainless steel, aluminum and glass). Figure 8.7 shows images of 0.6 mm diameter tin droplets impacting on a mirror-polished stainless steel substrate with 20 m/s velocity. Each column shows successive stages of droplet impact on a substrate at initial temperature ($T_{s,i}$) varying from 25°C to 200°C (indicated at the top of the column). The first picture in each sequence shows a droplet prior to impact, and the last shows the final splat shape. Droplets hitting a cold substrate ($T_{s,i} = 25°C$ –150°C) splashed extensively, producing small satellite droplets and leaving a splat with irregular edges. The extent of splashing decreased and eventually disappeared as substrate temperature was increased. No splashing was visible on a surface at 180°C. Solidification did not start until fairly late during spreading; localized freezing at several spots acted to obstruct spreading of the splat and produced an irregular shaped splat even though there was no splashing. At $T_{s,i} =$ 200°C solidification was sufficiently delayed that droplets spread to form thin discs. Computer simulations [42] have shown that freezing around the droplet periphery during spreading on a substrate at low temperature obstructs liquid flow and triggers splashing. When substrate temperature is increased, freezing is slowed down and the droplet spreads in the form of a thin liquid sheet without any splashing.

Dhiman and Chandra [20] developed an analytical model to predict the substrate temperature at which splashing would occur by using a one-dimensional model for solidification of a molten metal droplet in contact with a semi-infinite substrate. They assumed that splashing occurred if the thickness of the solid layer reached that of the splat by the time the droplet had finished spreading. The thermal contact resistance between the droplet and surface was found to play a critical role in

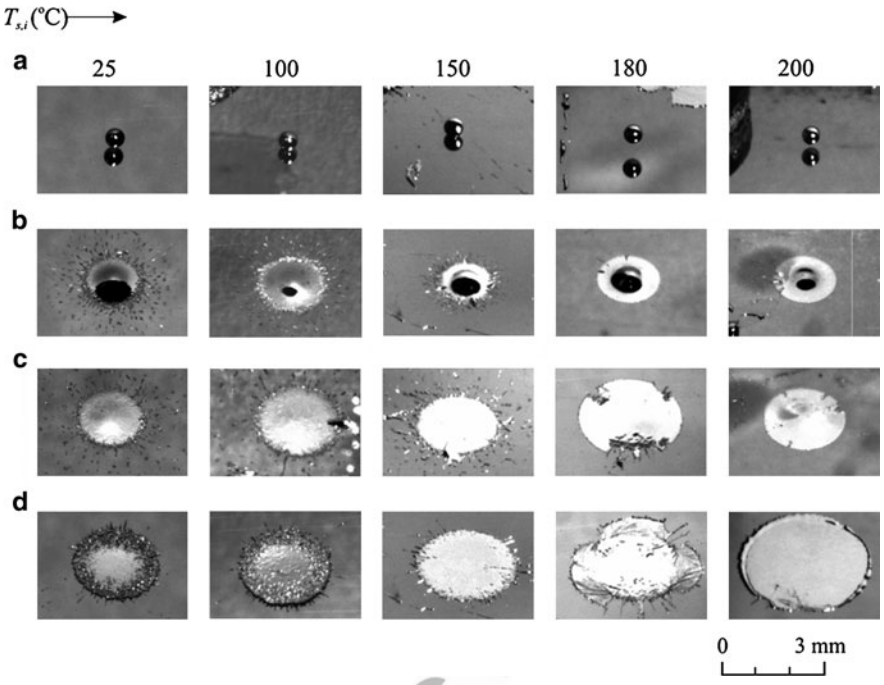


**Fig. 8.7** Impact of molten tin drops with velocity 20 m/s on a stainless steel surface at temperature, $T_{s,i}$ (1) 25°C, (2) 100°, (3) 150°C, (4) 180°C and (5) 200°C. The last picture in each column is the final solidified shape of the droplet. $Re = 43{,}636$, $We = 3{,}180$

determining whether splashing occurred, especially for high temperature melting point materials [43, 44]. Thermal resistance is created by imperfect contact at the droplet-substrate interface, and may be due to trapped air or the presence of contaminants such as adsorbed water vapor or oxide layers on the surface. The transition temperature at which splashing occurs therefore depends on the condition of the surface substrate.

## Droplet Rupture

Studies on splashing have largely focused on instabilities along the edges of the thin film created by the impacting droplet. Most of these studies have been conducted at relatively low impact velocities (1–10 m/s), where fluid instabilities around the edge of the spreading droplet caused the formation of long fingers that detached to form satellite droplets [3, 4]. At higher impact velocities, up to 40 m/s, photographs of water droplets impacting a polished stainless steel surface showed that the liquid became so thin that it ruptured internally and then, as the holes expanded due to surface tension the film disintegrated completely. Most practical spray applications

use high impact velocities and it is likely that a major cause of droplet break-up is internal rupture rather than edge instabilities.

Dhiman and Chandra [41] photographed impact of water droplets on surfaces of different wettability at impact velocities up to 30 m/s. Figure 8.8 shows three different sequences of the impact of water droplets on a wax surface at three different impact velocities: 10 m/s, 20 m/s and 30 m/s. Each vertical column shows successive stages of impact at one of the velocities, which yielded Reynolds numbers (*Re*) of 5,800, 11,600, and 17,400 respectively. Droplets flattened into a thin film after impact as they reached their maximum extension, followed by retraction until they eventually attained equilibrium. The diameter of the films at maximum extension increased with *Re* and hence their thickness decreased. Holes were formed in each film that grew larger, rendering the film unstable.

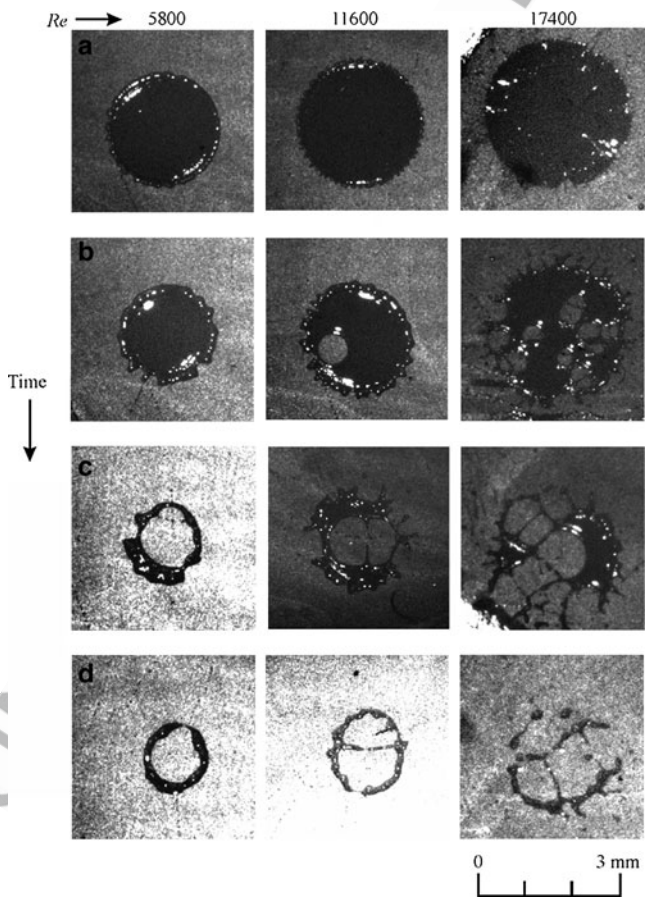


**Fig. 8.8** Impact of 580 μm diameter water droplets with different *Re* on smooth wax surfaces. Each column shows successive stages of impact [41]

Dhiman and Chandra [41] used a simple thermodynamic model to predict whether holes in a thin film would grow or not, comparing the surface energy of the intact liquid film resting on a surface with the energy of the same film with a hole in it. If the addition of the surface area of the hole decreased the total energy of the system, the hole would continue to grow, whereas, if it increased the energy the hole would close. In general, holes in a liquid film on a solid surface with very small or large contact angles have a large surface area and hence close up [41]. An intermediate contact angle produces a meniscus with small surface area, and such holes tend to expand. Experimentally, it was found that water films on hydrophilic or superhydrophobic surfaces remain stable, whereas those on surfaces with contact angles $\sim 90^\circ$ are the most likely to rupture.

For film rupture to commence a hole must be initiated in the liquid film. In practice, air bubbles trapped between the impacting droplet and substrate break through the liquid film and create holes. Increasing surface roughness promotes surface rupture since it increases the amount of air trapped at the interface. Similarly, raising the temperature of the substrate above the liquid boiling point also creates bubble and causes the film to fragment [45].



## References


1. A. M. Worthington: A study of splashes. Longmans, Green, London, 129 pp. (1908).
2. H. E. Edgerton, J. R. Killian: Flash! Seeing the unseen by ultra-high-speed photography. Branford, Boston, 215 pp. (1954).
3. S. D. Aziz, S. Chandra: Impact, recoil and splashing of molten metal droplets, Int. J. Heat Mass Transfer, 43, 2841–2857 (2000).
4. S. Chandra, P. Fauchais: Formation of solid splats during thermal spray deposition, J. Thermal Spray Technol., 18, 148–180 (2009).
5. R. Li, N. Ashgriz, S. Chandra, J. R. Andrews: Shape and surface texture of molten droplets deposited on cold surfaces, Surface Coatings Technol., 202, 3960–3966 (2008).
6. R. W. Gent, N. P. Dart, J. T. Cansdale: Aircraft icing, Philos. Trans. R. Soc. Lond. A, 358, 2873–2911 (2000).
7. L. Hulse-Smith, N. Z. Mehdizadeh, S. Chandra: Deducing droplet size and impact velocity from circular bloodstains, J. Forensic Sci., 50, 1–10 (2005).
8. M. Rein: Phenomena of liquid drop impact on solid and liquid surfaces, Fluid Dyn. Res., 12, 61–93 (1993).
9. A. L. Yarin: Drop impact dynamics: Splashing, spreading, receding, bouncing. . ., Annu. Rev. Fluid Mechanics, 38, 159–192 (2006).
10. C. D. Stow, M. G. Hadfield: An experimental investigation of fluid flow resulting from the impact of a water drop with an unyielding dry surface. Proc. R. Soc. Lond. Ser. A, 373, 419–441 (1981).
11. C. Mundo, M. Sommerfeld, C. Tropea: Droplet-wall collisions: experimental studies of the deformation and breakup process, Int. J. Multiphase Flow, 21, 151–173 (1995).
12. G. E. Cossali, A. Coghe, M. Marengo: The impact of a single drop on a wetted solid surface, Exp. Fluids, 22, 463–72 (1997).
13. K. Range, F. Feuillebois: Influence of surface roughness on liquid drop impact, J. Colloid Interface Sci., 203, 16–30 (1998).

14. R. L. Vander Wal, G. M. Berger, S. D. Mozes: The combined influence of a rough surface and thin fluid film upon the splashing threshold and splash dynamics of a droplet impacting onto them, Exp. Fluids, 40, 23–32 (2006).
15. M. Mani, S. Mandre, M. P. Brenner: Precursors to splashing of liquid droplets on a solid surface, Phys. Rev. Lett., 102, 134502 (2009).
16. M. Mani, S. Mandre, M. P. Brenner: Events before droplet splashing on a solid surface, J. Fluid Mech., 647, 163–185 (2010).
17. V. Mehdi-Nejad, J. Mostaghimi, S. Chandra: Air bubble entrapment under an impacting droplet, Phys. Fluids, 15, 173–183 (2003).
18. L. Xu, W. W. Zhang, S. R. Nagel: Drop splashing on a dry smooth surface, Phys. Rev. Lett., 94, 184505 (2005).
19. R. Rioboo, C. Tropea, M. Marengo: Outcomes from a drop impact on solid surfaces, Atomization Sprays, 11, 155–165 (2001).
20. R. Dhiman, S. Chandra: Freezing-induced splashing during impact of molten metal droplets with high Weber numbers, Int. J. Heat Mass Transfer, 48, 5625–5638 (2005).
21. N. Z. Mehdizadeh, S. Chandra, J. Mostaghimi: Formation of fingers around the edges of a drop hitting a metal plate with high velocity, J. Fluid Mechanics, 510, 353–373 (2004).
22. J. de Ruiter, R. E. Pepper, H. A. Stone: Thickness of the rim of an expanding lamella near the splash threshold, Phys. Fluids, 22, 022104 (2010).
23. C. Jossrand, L. Lemoyne, R. Troeger, S. Zaleski: Droplet impact on a dry surface: Triggering the splash with a small obstacle, J. Fluid Mechanics, 524, 47–56 (2005).
24. H. J. Subramani, T. Al-Housseiny, A. U. Chen, M. Li, O. A. Basaran: Dynamics of drop impact on a rectangular slot, Ind. Eng. Chem. Res., 46, 6105–6112 (2007).
25. L. Xu, L. Barcos, S. R. Nagel: Splashing of liquids: Interplay of surface roughness with surrounding gas, Phys. Rev. E, 76, 066311 (2007).
26. K. L. Pan, K. C. Tseng, C. H. Wang: Breakup of a droplet at high velocity impacting a solid surface, Exp. Fluids, 48, 143–156 (2010).
27. L. Xu: Liquid drop splashing on smooth, rough, and textured surfaces, Phys. Rev. E, 75, 056316 (2007).
28. P. Tsai, S. Pacheco, C. Pirat, L. Lefferts, D. Lohse: Drop impact upon micro- and nanostructured superhydrophobic surfaces, Langmuir, 25, 12293–12298 (2009).
29. R. D. Schroll, C. J. S. Zaleski, W. W. Zhang: Impact of a viscous liquid drop, Phys. Rev. Lett., 104, 034504 (2010).
30. G. E. Cossali, A. Coghe, M. Marengo The impact of a single drop on a wetted solid surface, Exp. Fluids, 22, 463–472 (1997).
31. G. E. Cossali, M. Marengo, A. Coghe, S. Zhdanov: The role of time in single drop splash on thin film, Exp. Fluids, 36, 888–900 (2004).
32. R. F. Allen: The role of surface tension in splashing, J. Coll. Interface Sci., 51, 350–351 (1975).
33. R. Bhola, S. Chandra: Parameters controlling solidification of molten wax droplets falling on a solid surface, J. Mater. Sci., 34, 4883–4894 (1999).
34. K. Range, F. Feuillebois: Influence of surface roughness on liquid drop impact, J. Colloid Interface Sci., 203, 16–30 (1998).
35. H. Y. Kim, Z. C. Feng, J. H. Chun: Instability of a liquid jet emerging from a droplet upon collision with a solid surface. Phys. Fluids, 12, 531–541 (2000).
36. A. I. Fedorchenko, A. A. Chernov: Formation of fingers at the front of an axially symmetric film of liquid upon the impact of a drop with a solid surface, Doklady Phys., 44, 570–572 (1999).
37. R. E. Pepper, L. Courbin, H. A. Stone: Splashing on elastic membranes: The importance of early-time dynamics, Phys. Fluids, 20, 082103 (2008).
38. S.T. Thoroddsen, J. Sakakibara: Evolution of the fingering pattern of an impacting drop, Phys. Fluids, 10, 1359–74 (1998).

39. S. S. Yoon, R. A. Jepsen, M. R. Nissen, T. J. O'Hern: Experimental investigation on splashing and nonlinear fingerlike instability of large water drops, J. Fluids Struct., 23, 101–115 (2007).
40. S. S. Yoon, R. A. Jepsen, S. C. James, J. Liu, G. Aguilar: Are drop-impact phenomena described by Rayleigh-Taylor or Kelvin-Helmholtz theory?, Drying Technol., 27, 316–321 (2009).
41. R. Dhiman, S. Chandra: Rupture of thin films formed during droplet impact, Proc. R. Soc. A, 466, 1229–1245 (2010).
42. N. Z. Mehdizadeh, M. Raessi, S. Chandra, J. Mostaghimi: Effect of substrate temperature on splashing of molten tin droplets, J. Heat Transfer, 126, 445–452 (2004).
43. A. McDonald, C. Moreau, S. Chandra: Thermal contact resistance between plasma sprayed particles and flat surfaces, Int. J. Heat Mass Transfer, 50, 1737–1749 (2007).
44. R. Dhiman, A. McDonald, S. Chandra: Predicting splat morphology in a thermal spray process, Surface Coatings Technol., 201, 7789–8801 (2007).
45. N. Z. Mehdizadeh, S. Chandra: Boiling during high velocity impact of water droplets on a hot stainless steel surface, Proc. R. Soc. Lond. A, 462, 3115–3131 (2006).

# Author Queries

Chapter No.: 8

| Query Refs. | Details Required | Author's response |
|---|---|---|
| Au1 | Please check if the edit to the abstract is OK. | |